JOURNAL OF CATALYSIS 144, 597–610 (1993)

Phase Equilibria and Butane Oxidation Studies of the $MgO–V_2O_5–MoO_3$ System

W. D. HARDING,*[,1] H. H. KUNG,*[,2] V. L. KOZHEVNIKOV,†[,3] AND K. R. POEPPELMEIER†[,2]

*Department of Chemical Engineering and Ipatieff Laboratory, and †Department of Chemistry and Ipatieff Laboratory, Northwestern University, Evanston, Illinois 60208-3113

Received February 22, 1992; revised July 13, 1993

Phase relations in the magnesium oxide-rich corner of the system $MgO–V_2O_5–MoO_3$ were studied. A new compound, $Mg_{2.5}VMoO_8$, was discovered. The solubility limit of molybdenum oxide in magnesium orthovanadate $Mg_{3-x}V_{2-2x}Mo_{2x}O_8$ was found to be $x \sim 0.03$. Butane oxidation studies of oxides with compositions along the pseudobinary line $Mg_3V_2O_8–Mg_{2.5}VMoO_8–MgMoO_4$ were investigated. All the compositions studied maintain the high catalytic dehydrogenation selectivity of the magnesium orthovanadate which is attributed to the similarities of vanadium environment in $Mg_{2.5}VMoO_8$ and $Mg_3V_2O_8$. Incorporation of molybdenum oxide in the orthovanadate results mainly in an increase of cracking products.

1. INTRODUCTION

Light alkanes are a potential feedstock to replace aromatics in a number of partial oxidation processes (*1*). However, selective oxidation of alkanes is among the most challenging catalytic problems because of their saturated chemical bonds. To date, only a small number of catalysts are known to be selective. Magnesium orthovanadate, $Mg_3V_2O_8$, has been found to be both active and selective in the oxidative dehydrogenation of butane and propane (2–4). Butenes and butadiene are the main products formed over a wide range of experimental conditions. Since molybdenum oxide is an essential component in the Bi–Mo oxide catalyst for the selective oxidation of propene to acrolein and in molybdates for the oxidation of butenes to maleic anhydride (*5, 6*), it becomes interesting to explore the effect of incorporating molybdenum oxide into $Mg_3V_2O_8$.

Substitution of Mo^{VI} into the V^V cation sites in magnesium orthovanadate should be possible because Mo^{VI} has a similar ionic radius and tetrahedral coordination as the V^V in magnesium orthovanadate. Its substitution could result in the reduction of V^V into V^{IV}, which is known to occur in mixed vanadium–molybdenum oxide (*7–9*). Alternatively, the excess charge of the molybdenum ion could be balanced by the generation of cation vacancies. In this paper, we report the subsolidus phase relations in the magnesium-rich region of the $MgO–V_2O_5–MoO_3$ system and compare the catalytic properties of a number of mixed oxides in the oxidation of butane.

2. EXPERIMENTAL

Standard solid-state procedures were used to study the phase relations among the constituent components MgO, V_2O_5, and MoO_3. Reagent grade oxides (Aldrich) were weighed in desired proportions, milled carefully with addition of ethanol and then cal-

[1] Current address: Department of Chemistry and Chemical Engineering, University of New Haven, West Haven CT.

[2] Correspondence should be addressed to either H. H. Kung or K. R. Poeppelmeier.

[3] Permanent address: Institute of Solid State Chemistry, Ural Branch of Academy of Sciences, 91 Pervomaiskaia, Yekaterinburg, Russia.

0021-9517/93 $5.00

cined at 600–650°C in a muffle furnace for 20–40 h with intermediate grindings. The firing temperature was then increased to 850–900°C and equilibration of specimens was performed for 60–100 h. Equilibria was assumed to be established when there were no further changes in the X-ray diffraction patterns. X-ray studies were carried out using a diffractometer (Rigaku Geigerflex) with Cu$K\alpha$ radiation.

Two aqueous methods were used to obtain specimens of higher surface areas for the butane oxidation studies. Solutions of ammonium metavanadate and ammonium heptamolybdate in hydrogen peroxide were mixed in appropriate proportions. These mixtures were added to appropriate quantities of an aqueous solution of magnesium nitrate, and the solutions were neutralized by ammonium hydroxide with rapid stirring. These precursors were fired slowly, increasing the temperature up to 550°C. The temperature was held at 550°C for ~100 h. X-ray diffraction showed only broad main reflections of the desired phase and no other peaks. The compositions $Mg_{2.97}V_{1.94}Mo_{0.06}O_8$ and $Mg_{2.5}VMoO_8$ obtained by this procedure were used in catalytic tests. They had surface areas of 7.5 and 6.4 m^2/g, respectively, as measured by N_2 BET. Small portions of each composition when heated at ~900°C formed well crystallized powders of the desired compounds. The compositions $Mg_3V_2O_8$, $Mg_{2.9}V_{1.8}Mo_{0.2}O_8$ and $Mg_{2.75}V_{1.5}Mo_{0.5}O_8$ were prepared by a slightly different procedure to achieve higher surface areas. Namely, high surface area magnesium oxide was prepared by thermal decomposition of $Mg(OH)_2$ by ramping the temperature from 100 to 450°C over a period of 8 h. The measured BET surface area of the resulting MgO was in the range of 110–180 m^2/g. Ammonium metavanadate and/or ammonium heptamolybdate were dissolved in deionized water with addition of ammonium hydroxide. Magnesium oxide was then added to the solution to form a suspension, which was evaporated to dryness. The solid was then ground and calcined at 550°C for 6 h. X-ray diffraction detected the presence of the desired phases. The resulting solid catalysts of compositions $Mg_3V_2O_8$, $Mg_{2.9}V_{1.8}Mo_{0.2}O_8$, and $Mg_{2.75}V_{1.5}Mo_{0.5}O_8$ had surface areas of 54, 26, and 15 m^2/g, respectively.

The reaction studies were carried out in quartz tube downflow reactors. The reaction mixture consisted of 86 vol% helium (Linde, High Purity Grade), 2 vol% nitrogen (Linde, High Purity Grade), 8 vol% oxygen (Linde, Extra Dry Grade), and 4 vol% butane (Linde, CP Grade). The helium and nitrogen were from a custom-mixed gas. The nitrogen was used as an inert tie component to improve material balance during the reaction runs. Precise flow rates were maintained by mass flow controllers. Quartz chips were used to fill the volumes both before and after the catalyst bed to minimize potential gas-phase pyrolysis reactions particularly at the higher reaction temperatures. Pyrolysis was determined to be negligible in all the experiments performed. A quartz thermowell was inserted into the catalyst bed to monitor the internal bed temperature. The reactor temperature was controlled by a thermocouple attached to the exterior of the reactor.

The feed mixture was analyzed by gas chromatography using TC detectors, a molecular sieve 13X column and a VZ-7 (Alltech) column. The product stream was first sampled and injected to a Carbowax 20M on Graphpac GB column to separate hydrocarbons and oxygenated components. The product stream then passed through a trap maintained at 0°C to remove any condensible components. It was then sampled by a second product sampled loop for analysis utilizing the same GC columns as for the feed mixture.

Reactions were run over the temperature range 400–540°C. Conversion of butane at a particular temperature was controlled by varying the total flow rate of reactant mixture or by varying the amount of catalyst used.

3. PHASE RELATIONS IN MgO-RICH CORNER OF THE SYSTEM $MgO-V_2O_5-MoO_3$

When molybdenum oxide was substituted into magnesium orthovanadate according to the formula $Mg_3V_{2-x}Mo_xO_8$ with $x = 0.2$ and 0.5 single-phase materials were not obtained. To clarify phase constituents in these compositions we used systematic triangulation. Compositions along the lines from the point $MgO : V_2O_5 = 3 : 1$ (orthovanadate) of the binary system $MgO-V_2O_5$ to the points of the binary system $MgO-MoO_3$ with ratios $MgO : MoO_3 = 1 : 1, 1.5 : 1, 2 : 1, 3 : 1, 4 : 1$ were investigated. All of these samples showed the presence of an unidentified phase in combination with magnesium orthovanadate ($Mg_3V_2O_8$) or magnesium molybdate ($MgMoO_4$) depending on the composition. The X-ray diffraction patterns of the specimens along the line $Mg_3V_2O_8$–$MgMoO_4$ with bulk composition $Mg_{3-x}V_{2-2x}Mo_{2x}O_8$ are shown in Fig. 1. These data definitely point out the existence of two solid phases between the points $0 < x < 0.5$ and $0.5 < x < 1.0$. Additional experiments also showed the equilibrium between MgO and $Mg_{3-x}V_{2-2x}Mo_{2x}O_8$ with $x = 0.5$. The firing of the oxide mixture $MgO : V_2O_5 : MoO_3 = 7 : 2 : 1$, corresponding to the triangle $Mg_3V_2O_8$–$Mg_2V_2O_7$–$Mg_{2.5}VMoO_8$, gives three phases in equilibrium between the constituent points. These results suggest that the singular point $Mg_{2.5}VMoO_8$ corresponds to an individual compound.

The X-ray spectrum of the compound $Mg_{2.5}VMoO_8$ was indexed with the orthorhombic cell parameters $a = 10.344 \pm 0.003$ Å, $b = 17.468 \pm 0.005$ Å, and $c = 5.057 \pm 0.002$ Å. The main diffraction peaks, their intensities, and a comparison of experimental and calculated lattice spacings are presented in Table 1. This spectrum corresponds very well to the diffraction pattern of $Li_2Ni_2Mo_3O_{12}$ described by Ozima *et al.* (*10*). The main features of the structure of $Li_2Ni_2Mo_3O_{12}$ (see Fig. 2) are molybdenum in tetrahedral coordination, and the presence of three inequivalent positions for (Li, Ni) that are coordinated by six oxygen atoms. It is interesting to point out that two distorted octahedral positions denoted as $M2$ and $M3$ are shared by lithium and nickel cations and closely linked via their edges and molybdenum tetrahedra, but the third position denoted as $M1$, having a trigonal prismatic oxygen environment, is occupied by lithium ions only. The lithium ions in this position form chains along the [001] direction, and they have the longest average distance to oxygen neighbors. This indicates a weaker bonding with the crystalline lattice for the ions residing in the $M1$ positions.

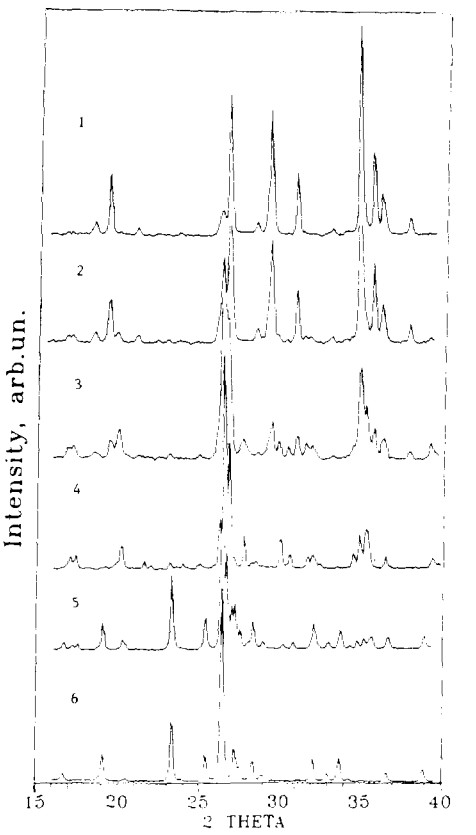

FIG. 1. X-ray diffraction patterns of composition $Mg_{3-x}V_{2-2x}Mo_{2x}O_8$. Samples calcined in air at 900°C. $x = 0.03$ (1), 0.09 (2), 0.33 (3), 0.5 (4), 0.75 (5), and 1.00 (6).

In $Mg_{2.5}VMoO_8$, magnesium cations presumably reside in all three positions $M1$, $M2$ and $M3$. However, owing to the coexistence

TABLE 1

X-ray data for $Mg_{2.5}VMoO_8$

N	h	k	l	I/I_0	D(obs), Å	D(calc), Å[a]
1	2	0	0	8.1	5.1712	5.1720
2	1	3	0	7.0	5.0702	5.0740
	0	0	1			5.0568
3	1	1	1	18.1	4.3876	4.3968
	0	2	1			4.3763
4	0	3	1	6.3	3.8196	3.8180
5	3	1	0	23.2	3.3758	3.3827
6	2	2	1	100	3.3380	3.3408
	2	4	0			3.3367
7	1	5	0	51.2	3.3031	3.3099
	0	4	1			3.3051
8	3	3	0	8.1	2.9635	2.9668
9	0	6	0	6.3	2.9085	2.9113
10	3	1	1	7.3	2.8083	2.8116
11	2	4	1	7.3	2.7827	2.7850
12	4	0	0	6.2	2.5850	2.5860
13	3	3	1	15.7	2.5577	2.5589
	4	1	0			2.5581
14	0	0	2	18.8	2.5269	2.5284
	0	6	1			2.5231
15	3	5	0	5.6	2.4520	2.4541
	1	6	1			2.4521
16	4	1	1	6.3	2.2832	2.2827
17	2	6	1	4.0	2.2678	2.2676
18	3	3	2	8.0	1.9261	1.9244
19	0	6	2	8.0	1.9073	1.9090
	1	9	0			1.9076
20	5	2	1	6.3	1.8710	1.8703
	5	4	0			1.8696
	2	8	1			1.8691
21	4	0	2	11.3	1.8080	1.8079
22	2	6	2	10.9	1.7913	1.7909
23	1	9	1	7.3	1.7834	1.7848

[a] Calculated with orthorhombic cell parameters, $a = 10.344 \pm 0.003$ Å, $b = 17.468 \pm 0.005$ Å, $c = 5.057 \pm 0.002$ Å; two reflections with $d > 5.2$ Å $hkl = 020$ ($d \sim 8.7$ Å) and $hkl = 110$ ($d \sim 8.9$ Å) were also observed.

of pentavalent vanadium and hexavalent molybdenum, one sixteenth of the magnesium positions are empty. This can be seen when comparing the balance of atoms in the compounds written in the forms $Mg_{15}V_6Mo_6O_{48}$ and $Li_8Ni_8Mo_{12}O_{48}$. The above considerations indicate that the most probable location of these cation vacancies is in the *M1* positions. The vanadium and molybdenum cations are located in oxygen tetrahedra. These tetrahedra are isolated in the crystalline framework. Hence, the coordination of the transition metal cations and the linkage pattern of the tetrahedra containing the transition metal via octahedra containing the magnesium cation, resemble structural features found in the compound $Mg_3V_2O_8$. The general resemblance is reflected in some similarity of the X-ray spectra of these compounds, for example, the presence of the groups of strong reflections at 26–27° and 35–37° (2Θ) (Fig. 1). A more detailed description of the crystalline structure and properties of the $Mg_{2.5}VMoO_8$ will be presented in a separate publication.

The experimental data show that MoO_3 is soluble in magnesium orthovanadate up to 0.03 mole fraction. Figure 3 shows the elementary cell parameters of $Mg_{3-x}V_{2-2x}Mo_{2x}O_8$ with small concentrations of molybdenum cations estimated from the (132), (023), (113) diffractions referenced to those of orthorhombic magnesium orthovanadate. The lattice parameters obtained for pure, undoped $Mg_3V_2O_8$ are slightly smaller than the JCPDS-ICDD data that were refined for a monocrystalline sample. This difference is most likely due to the sample's imperfection (strains, defects, etc.). From the changes of lattice parameters for the doped series, one can estimate the solubility limit at $x \sim 0.03$. It is interesting to note that the color of the sample with $x \sim 0.03$ is off-white or light yellow, indicating the absence of defect centers containing tetravalent vanadium. One explanation for this is the formation of cation vacancies at magnesium sites with molybdenum incorporation into the matrix compound rather than a change of vanadium oxidation state. The data obtained allow us to construct the phase equilibrium diagram in the magnesium-rich corner of the system $MgO–V_2O_5–MoO_3$, shown in Fig. 4. The elementary triangles are $MgO–Mg_3V_2O_8–Mg_{2.5}VMoO_8$; $MgO–Mg_{2.5}VMoO_8–MgMoO_4$; $Mg_3V_2O_8–Mg_2V_2O_7–Mg_{2.5}VMoO_8$; and $Mg_2V_2O_7–Mg_{2.5}VMoO_8–MgMoO_4$.

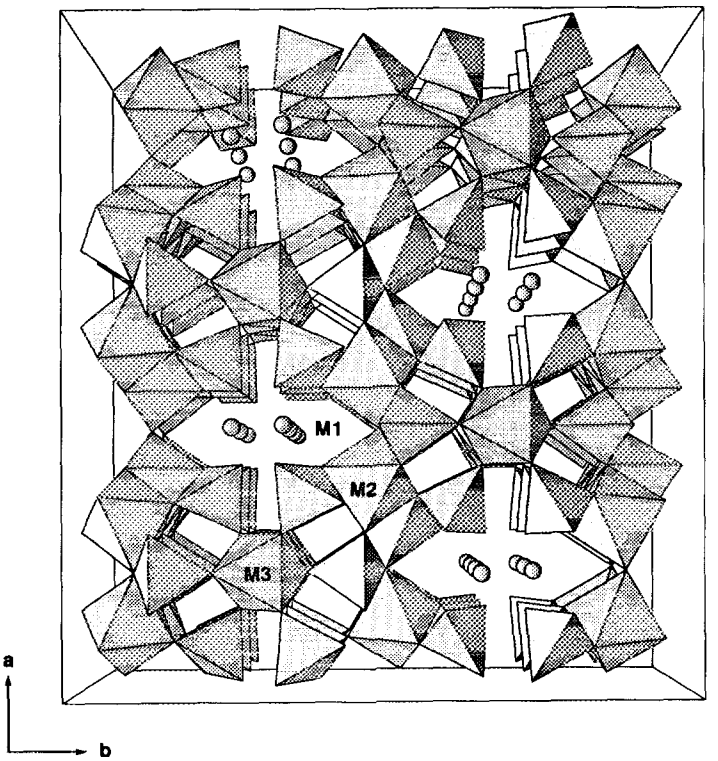

FIG. 2. The [001] projection of the structure of $Mg_{2.5}VMoO_8$, (structure analog is $Li_2Ni_2Mo_3O_{12}$). Positions *M*1, *M*2, and *M*3 are shown.

The X-ray spectra, of several $Mg_{3-x}V_{2-2x}Mo_{2x}O_8$ specimens obtained *at low temperature*, are presented in Fig. 5. That for sample $x = 0.03$ showed the strong triplet of peaks in the vicinity of 35–37° (2Θ) which is characteristic for the magnesium orthovanadate. The sample $x = 0.50$ showed the presence of a strong broad line around 27° (2Θ) which can be attributed to the phase $Mg_{2.5}VMoO_8$ (compare with Fig. 1). The X-ray spectrum of sample $x = 0.25$ can be interpreted as a mixture of phases

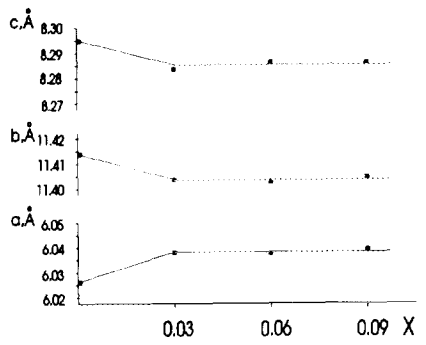

FIG. 3. Lattice parameters of $Mg_{3-x}V_{2-2x}Mo_{2x}O_8$.

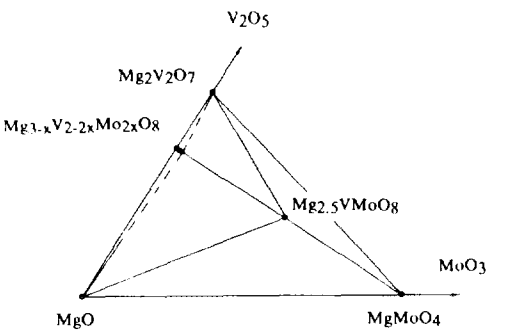

FIG. 4. Phase equilibria in triangle $MgO-Mg_2V_2O_7-MgMoO_4$. Samples calcined at 900°C in air.

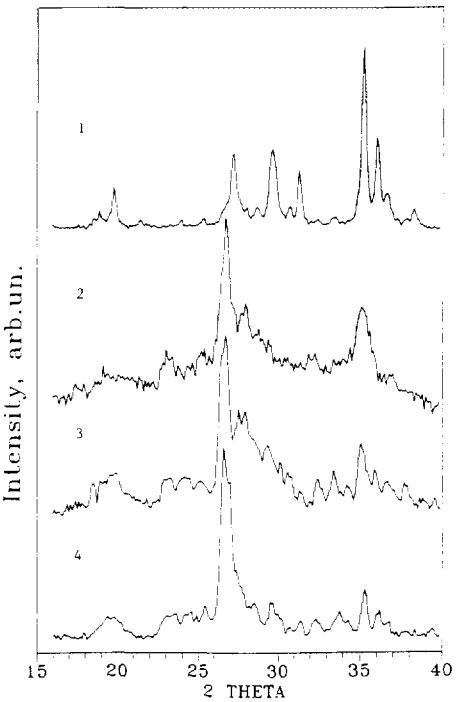

FIG. 5. X-ray spectra of the samples $Mg_{3-x}V_{2-2x}Mo_{2x}O_8$ obtained at 550°C. $x = 0.03$, 100 h (1); 0.25, 6 h (2); 0.25, 100 h (3); and 0.50, 100 h (4).

for $x = 0.03$ and $x = 0.5$. A comparison of the spectra of the specimens obtained during short time (6 h) and long time (100 h) (curves 2 and 3, respectively) heat treatment at 550°C did not reveal significant differences. Therefore, one can conclude that the phase relations at ~550°C are the same as at ~900°C. The aqueous preparation allowed us to obtain more dispersed individual compounds or their mixtures without changing the phase relations in the system under study. The use of longer calcination time or higher temperature leads only to the decrease of surface area and the formation of more well-shaped microcrystals in the powder specimen, as shown in Figs. 6 and 7.

Figure 7 shows the typical morphology of the powder specimens $Mg_{2-x}V_{2-2x}Mo_{2x}O_8$ obtained at 500°C. The powder consists of rolls with average dimensions 10–30 μm, Figs. 7a and 7b. These rolls are agglomerated from smaller poorly shaped particles of nearly spherical form and which have rather uniformly distributed sizes around 0.1 μm, Fig. 7c.

Laser Raman spectroscopy was performed on several low temperature samples of the composition $Mg_{3-x}V_{2-2x}Mo_{2x}O_8$ to provide information concerning the metal-oxygen bonding and vanadium and molybdenum environment. These spectra are shown in Fig. 8. The two end-point compounds studied were $Mg_3V_2O_8$ ($x = 0$) and $MgMoO_4$ ($x = 1$) (curves 1 and 6, respectively). The spectrum of $Mg_{2.5}VMoO_8$ ($x = 0.5$) is close to a linear combination of these two. This is expected considering the similarity in the structures of the three compounds and the fact that the intermediate compound maintains many of the structural characteristics of the end point compounds as is shown by the X-ray patterns in Fig. 1. For example, vanadium and molybdenum are found in tetrahedral coordination in their respective end point compounds as well as in the intermediate compound as discussed earlier. The spectra obtained here for $Mg_3V_2O_8$ and $MgMoO_4$ compare well with those reported (*11*, *12*). The bands at 870 and 834 cm^{-1} for the $x = 0$ compound have been assigned to VO_4 asymmetric stretch (*11*). For the $x = 1$ compound, the 976- and 965-cm^{-1} bands may be assigned to Mo–O bond stretching (*12*). Raman bands at lower frequencies are generally associated with group stretching modes or bending modes. The spectra obtained for the mixtures ($x = 0.1$, 0.25) are consistent with the fact that they are a mixture of phases.

4. REACTION STUDY

The catalytic behavior of several compositions corresponding to the formula $Mg_{3-x}V_{2-2x}Mo_{2x}O_8$ ($x = 0$, 0.03, 0.1, 0.25, and 0.5) was investigated in the oxidation of butane. According to the results of the phase relationship analysis, the samples of $x = 0.5$ and 0.03 corresponded to an individual compound and the solubility limit of the solid solution based on orthovanadate, re-

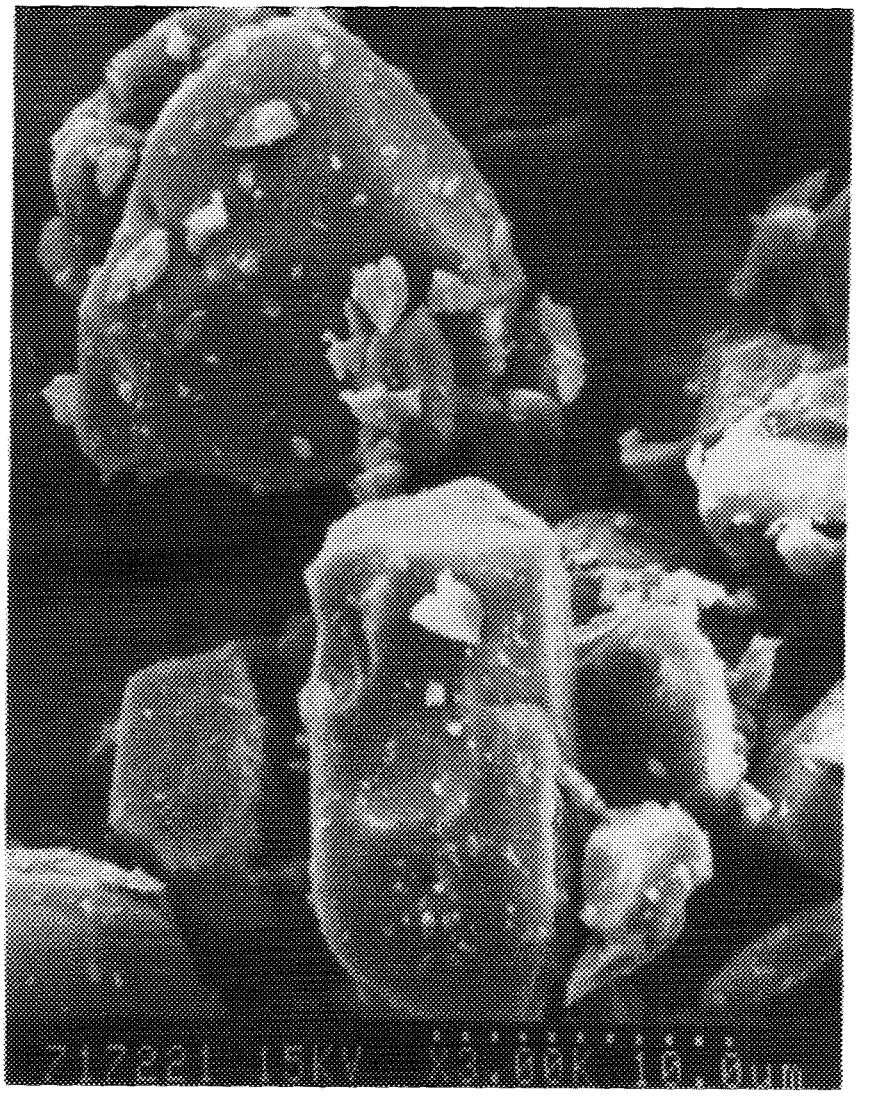

FIG. 6. SEM micrograph of the magnesium orthovanadate calcined for 100 h at 950°C. Magnification $\times 3000$.

spectively. The samples of $x = 0.1$ and 0.25 represented 20 and 50 mol% of $Mg_{2.5}VMoO_8$ in $Mg_3V_2O_8$, respectively. All of the samples tested were effective in the oxidative dehydrogenation of butane to 1-butene, *cis*-2-butene, *trans*-2-butene, and butadiene. For the comparison of the samples, the total dehydrogenation selectivity (TDS), which is the sum of the selectivities to the three butene isomers and to butadiene is reported, in addition to the individual products.

Figures 9–11 show the variation of TDS with butane conversion. At each temperature, the conversion was varied by changing the W/F ratio. TDS was observed to decrease with increasing conversion at all reaction temperatures and increased with reaction temperature at a fixed butane conversion, as is illustrated in Fig. 9 for

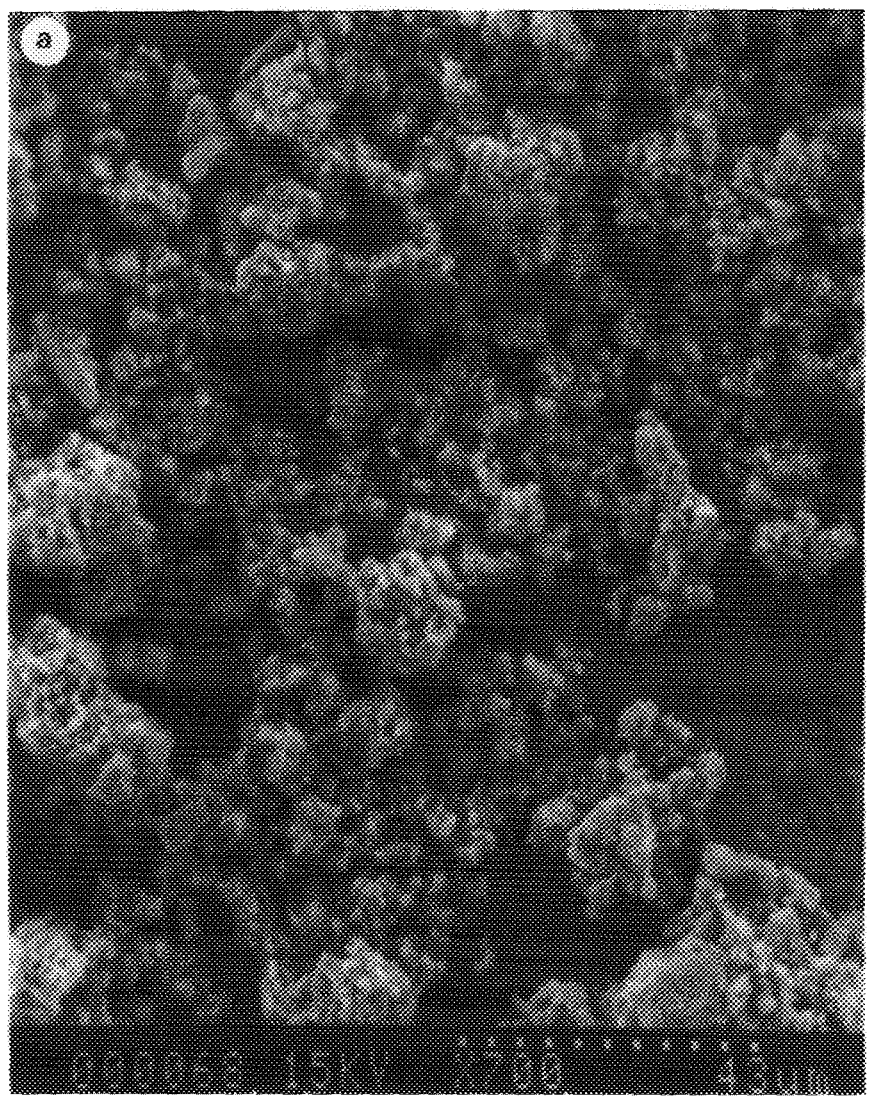

FIG. 7. SEM micrographs of $Mg_{3-x}V_{2-2x}Mo_{2x}O_8$, $x = 0.25$, calcined for 100 h at 550°C. Magnification: (a) ×700, (b) ×3400, and (c) ×19,800.

$Mg_{2.9}V_{1.8}Mo_{0.2}O_8$ ($x = 0.1$). At 10% butane conversion, the TDS increased from ~43% at 400°C to ~73% at 540°C. This same trend was also observed for the $Mg_3V_2O_8$ ($x = 0.00$), $Mg_{2.75}V_{1.5}Mo_{0.5}O_8$ ($x = 0.25$), and $Mg_{2.5}VMoO_8$ ($x = 0.50$) catalysts, as can be seen in Table 2. For magnesium orthovanadate, these same trends can also be inferred from data presented by Chaar *et al.* (*2, 13*). In addition, by comparing different catalyst compositions at the same reaction temperature and considering the scatter of the data, it was found that TDS did not vary substantially with composition. This is particularly so for reaction at 500°C (Fig. 10) where data for all compositions appear to follow the same trend. At 540°C (Fig. 11), there was a slightly bigger spread of TDS which was more evident at higher conversions. This may be due in part to an increased selectiv-

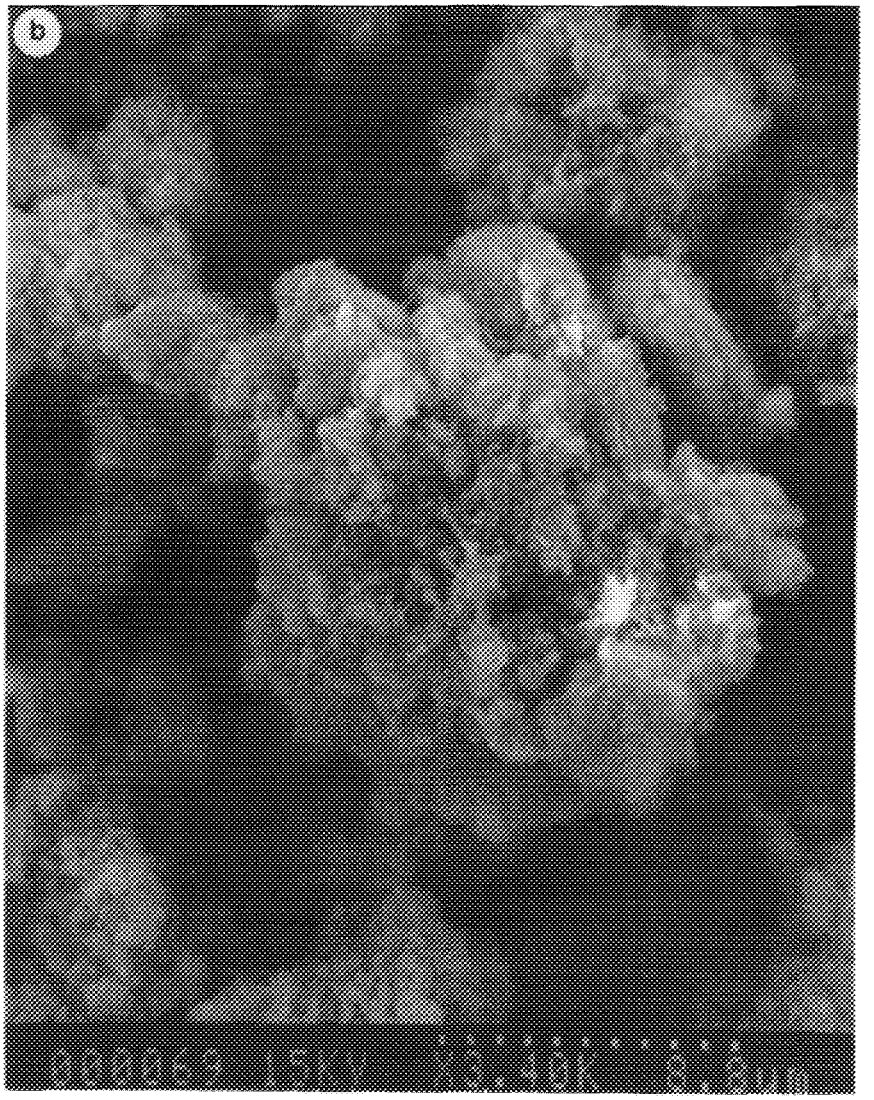

FIG. 7—*Continued*

ity to cracked products with the incorporation of molybdenum, as discussed later.

Although the TDS at the lower temperature appeared to be similar on the different catalysts, the selectivity for butadiene and correspondingly the selectivities for butenes, differed. Magnesium orthovanadate produces a higher proportion of butadiene than the molybdenum-containing samples under all conditions studied, when the catalysts were compared at the same temperature and conversions. This trend is easily observed at 540°C, as shown in Fig. 12 which compares the fraction of dehydrogenation products accounted for by butadiene for the various compositions studied. The compositions with $x = 0.03$, $x = 0.1$, and $x = 0.25$ showed similar fractions of butadiene, and the orthovanadate exhibited roughly 10% higher fractional selectivity.

The fraction of dehydrogenation product being butadiene increased with increasing

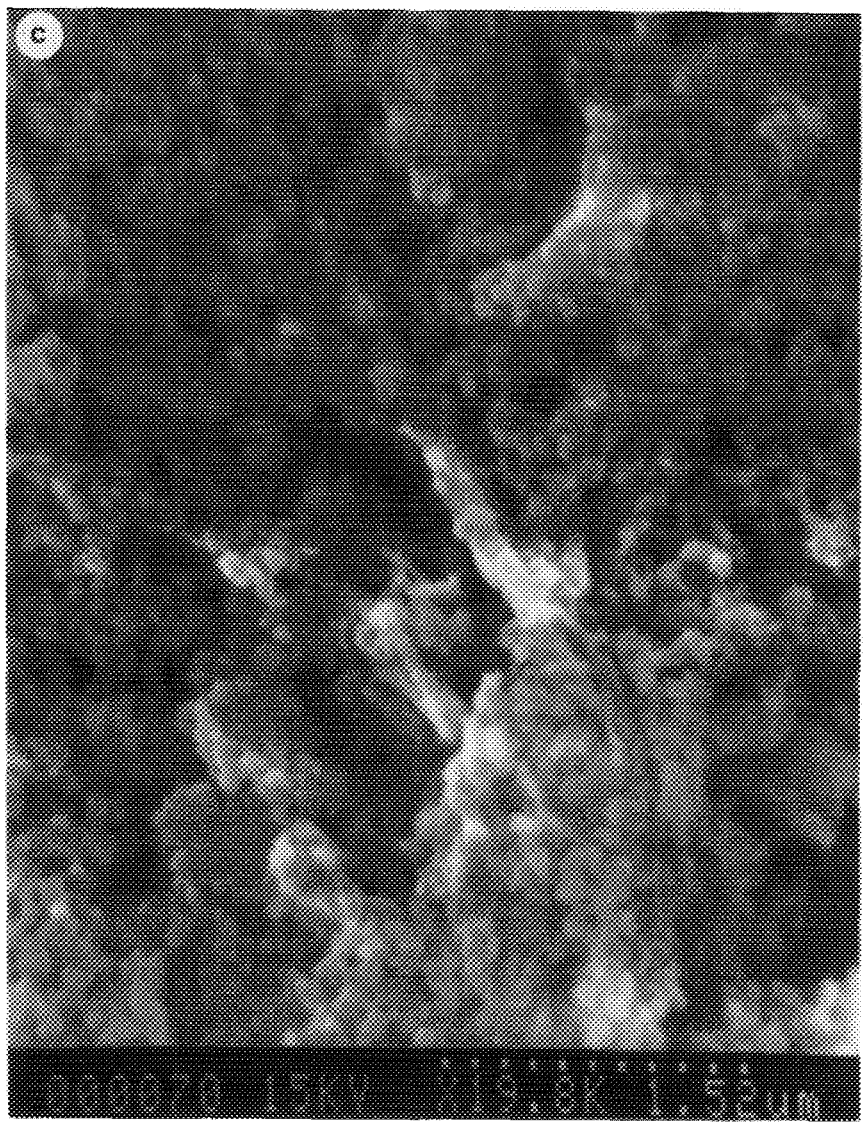

FIG. 7—*Continued*

conversion for all temperatures and also increased with reaction temperature at a given conversion. This is shown for the sample of $x = 0.1$ in Table 3. For all compositions, the fractional selectivity to butadiene increased with increasing conversion, as shown in Fig. 12. This trend, coupled with the trend of decreasing TDS with increasing conversion, is likely due to an increasing extent of successive reactions in the consecutive reaction scheme: butane to butenes to butadiene to carbon oxides (*13*). The observed decrease in selectivity to butadiene with increasing molybdenum content could be due to some type of inhibition of the conversion of butene to butadiene. However, it has been observed previously in our laboratory that there seems to be an increase in the selectivity to butadiene with an increase in catalyst surface area. This would follow

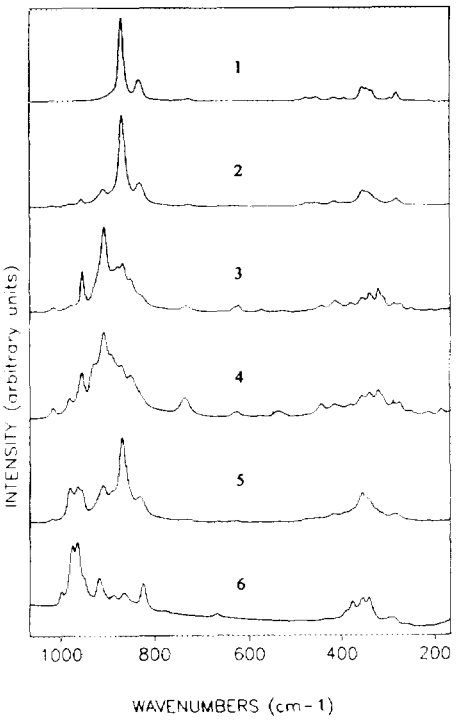

FIG. 8. The Raman spectra of the samples along the line $Mg_3V_2O_8$–$Mg_{2.5}VMoO_8$ obtained by calcining at 550°C for 100 h. x = 0.00 (1), 0.03 (2), 0.10 (3), 0.25 (4), 0.50 (5), and 1.00 (6).

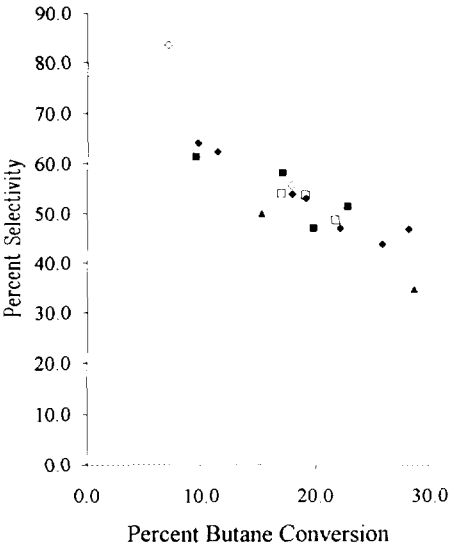

FIG. 10. Total dehydrogenation selectivity versus butane conversion for $Mg_{3-x}V_{2-2x}Mo_{2x}O_8$ at 500°C. x = 0 (■), 0.03 (□), 0.1 (◆), 0.25 (◇), and 0.5 (▲).

from the reactants having a longer residence time in the catalyst pores and thus a higher probability of butene reabsorbing onto the catalyst surface and being converted to bu-

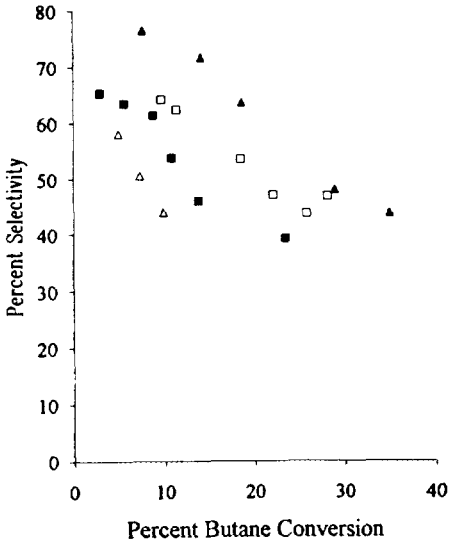

FIG. 9. Total dehydrogenation selectivity versus butane conversion for $Mg_{3-x}V_{2-2x}Mo_{2x}O_8$ (x = 0.1) at 400°C (△), 450°C (■), 500°C (□), and 540°C (▲).

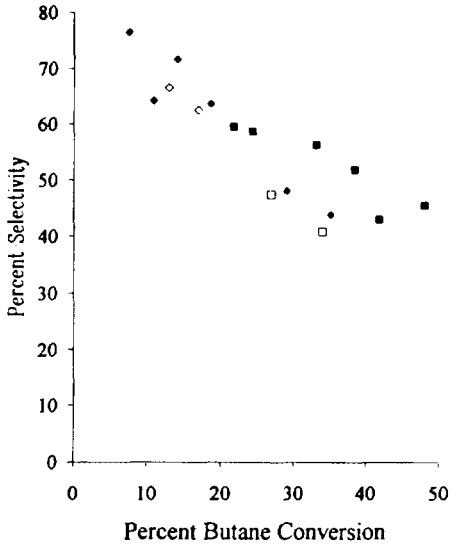

FIG. 11. Total dehydrogenation selectivity versus butane conversion for $Mg_{3-x}V_{2-2x}Mo_{2x}O_8$ at 540°C. x = 0 (■), 0.03 (□), 0.1 (◆), and 0.25 (◇).

TABLE 2

Sample Product Distributions Showing Selectivities for Dehydrogenation Products, Carbon Oxides, and Cracked Products with Temperature and Composition of Catalysts in Butane Oxidation

Catalyst	T(°C)	$\frac{W}{F}\left(\frac{\text{g min}}{\text{liter}}\right)$	Conversion (%)	Selectivities (%)								Ratio[b] 2-butene / 1 butene
				1-Butene	*trans*-2-Butene	*cis*-2-Butene	Butadiene	Total dehydrogenation	CO	CO_2	Cracked products[a]	
$Mg_3V_2O_8$	450	3.1	10.9	12.3	7.2	8.7	4.4	32.6	13.7	53.8	0.0	1.3
	500	1.0	9.5	22.3	12.3	13.8	13.0	61.4	10.2	28.3	0.0	1.2
	500	2.0	22.8	17.3	8.5	9.8	15.8	51.4	11.4	37.2	0.0	1.1
	540	1.0	21.7	18.2	6.3	8.0	26.9	59.4	10.2	26.8	3.5	0.8
$Mg_{2.9}V_{1.8}Mo_{0.2}O_8$	450	20	23.4	10.5	11.2	10.5	7.1	39.3	20.0	37.0	3.7	2.1
	500	10	22.1	11.6	11.8	9.8	13.8	47.0	18.8	28.5	5.7	1.9
	540	3.4	18.5	18.6	16.3	13.7	16.8	65.4	10.7	13.6	10.4	1.6
$Mg_{2.75}V_{1.5}Mo_{0.5}O_8$	450	8.0	8.0	15.1	18.2	21.4	6.9	62.1	9.9	25.8	2.3	2.6
	500	5.2	7.1	19.9	19.7	24.4	19.6	83.6	5.8	9.0	1.6	2.2
	500	7.8	17.9	13.7	13.8	11.6	16.4	55.5	12.8	24.2	7.5	1.9
	540	6.7	16.9	19.0	13.2	13.9	16.4	62.5	13.3	20.0	4.3	1.4
$Mg_{2.5}VMoO_8$	450	32	14.5	12.6	10.7	10.2	10.8	44.3	19.9	33.8	2.0	1.7
	500	16	15.3	14.5	10.8	10.7	14.1	50.1	20.9	25.2	3.9	1.5

[a] Cracked products indicates the sum of ethene and propene generated from cracking of the C_4 chain.
[b] Ratio of (*cis*-2-butene + *trans*-2-butene) to 1-butene.

tadiene. The current data are consistent with either explanation since the decrease in surface areas of the various catalysts also correlates reasonably well with the decrease in butadiene/butene ratio.

With the addition of molybdenum to magnesium orthovanadate, a substantial increase in the production of cracked products was observed, which included ethene and propene that were formed by breaking of the C_4 chain. For a given reaction temperature and butane conversion, the selectivity to cracked products increased substantially with increasing x. As shown in Fig. 13, at 540°C, the compositions that were low in molybdenum (x = 0 and 0.03) produced between 3 and 5% cracked products, while the compositions with higher molybdenum content (x = 0.1 and 0.25) produced between 8 and 10% cracked products. This may be due to increased acidity from the addition of molybdenum to the matrix as acidity is known to enhance cracking (*14*). This increased selectivity to cracked products with molybdenum addition may also account for the variation of TDS selectivity at 540°C for the molybdenum-containing compounds as was observed in Fig. 11. The selectivity to carbon oxides was observed to be almost constant with varying molybdenum content at 540°C, indicating that the sum of dehydrogenation selectivity and cracking selectivity was almost constant. The ratio of the total 2-butene selectivity to

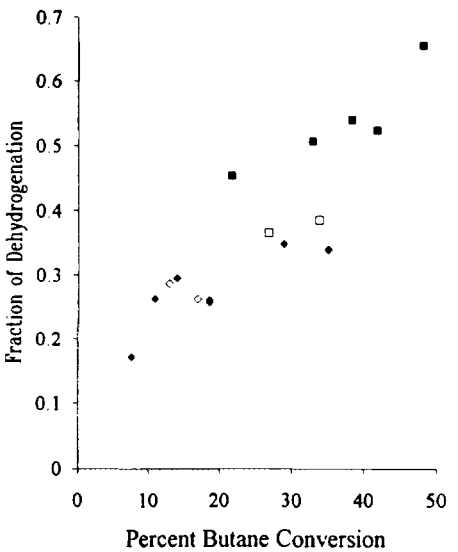

FIG. 12. Fractional selectivities to butadiene for $Mg_{3-x}V_{2-2x}Mo_{2x}O_8$ at 540°C. x = 0 (■), 0.03 (□), 0.1 (◆), and 0.25 (◇).

TABLE 3

Fraction of Dehydrogenation Product Accounted for by Butadiene versus Conversion for $Mg_{2.9}V_{1.8}Mo_{0.2}O_8$

Temperature (°C)	Conversion (%)	Fraction of dehydrogenation product being butadiene	Selective to butadiene (%)	TDS (%)
400	4.9	0.086	5.0	58.1
400	9.9	0.139	6.1	44.0
450	5.8	0.161	10.2	63.3
450	8.3	0.175	10.8	61.7
450	23.4	0.181	7.1	39.3
500	10.8	0.185	11.7	62.9
500	18.4	0.249	13.3	53.5
500	28.1	0.267	12.5	46.8
540	9.3	0.217	15.0	70.4
540	18.6	0.259	16.5	63.6
540	28.9	0.348	16.7	48.0

the 1-butene selectivity was also found to increase with the increase in the MoO_3 content of the catalysts. This trend is consistent with the proposed increase in catalyst acidity with increasing molybdenum content as isomerization of butenes is well known to be acid catalyzed (*14*).

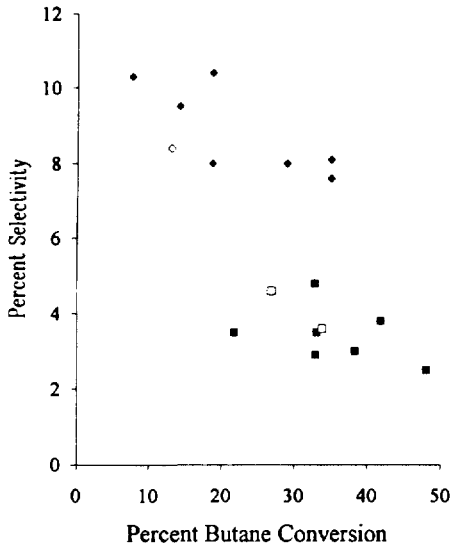

FIG. 13. Selectivity to cracked products for $Mg_{3-x}V_{2-2x}Mo_{2x}O_8$ at 540°C. x = 0 (■), 0.03 (□), 0.1 (◆), and 0.25 (◇).

5. CONCLUSION

Substitution of molybdenum oxide in the crystalline lattice of magnesium orthovanadate led to the formation of defects in the magnesium sublattice according to the formula $Mg_{3-x}V_{2-2x}Mo_{2x}O_8$, such that the oxidation state of vanadium remained unchanged. The structure of magnesium orthovanadate was stable only when the sample had rather low concentrations of magnesium vacancies ($x < 0.03$). At higher concentrations of vacancies, the crystalline lattice rearranged into a new structure, that of $Mg_{2.5}VMoO_8$. The essential resemblance of this structure to the structure of magnesium orthovanadate was the conservation of tetrahedral vanadium coordination and isolation of the vanadium tetrahedra from one another. As was suggested by Chaar *et al.* (*2*), these properties of the magnesium orthovanadate crystalline lattice were responsible, in general, for its catalytic behavior. The butane oxidation results obtained showed that, indeed, $Mg_{2.5}VMoO_8$, $Mg_{2.97}V_{1.94}Mo_{0.06}O_8$, or their "self supported" mixtures showed catalytic behavior that closely resembled that of magnesium orthovanadate.

The crystalline structure of the compound $Mg_{2.5}VMoO_8$ is more versatile compared

with the structure of $Mg_3V_2O_8$ in that it is more flexible for isomorphous substitutions compared to the rather rigid crystalline lattice of the orthovanadate. Preliminary experiments have shown that incorporation of other ions on the magnesium and the vanadium sublattices occurs over rather wide limits. These isomorphous substitutions influence not only the defect structure of the compound, but its acidity also, making further investigations of the catalytic behavior of the compositions based on $Mg_{2.5}VMoO_8$ quite promising. This work is in progress and results will be reported in a future communication.

ACKNOWLEDGMENTS

The authors acknowledge an Extramural Research Award (EMRA) from BP America, Inc., for support of this research. The surface area equipment was made possible by the Department of Energy, Contract DE-F605-86ER75295. This research made use of MRL Central Facilities supported by the National Science Foundation, at the Materials Research Center of Northwestern University, under Award DMR-9120521.

REFERENCES

1. Snyder, T. P., and Hill, C. G. Jr., *Catal. Rev.-Sci. Eng.* **31,** 43 (1989).
2. Charr, M. A., Patel, D., Kung, M. C., and Kung, H. H., *J. Catal.* **105,** 483 (1987).
3. Patel, D., Kung, M. C., and Kung, H. H., *in* "Proceedings, 9th International Congress on Catalysis, Calgary, 1988" (M. J. Phillips and M. Ternan, Eds.), Vol. 4, p. 1554. Chem. Inst. of Canada, Ottawa, 1988.
4. Seshan, K., Swaan, H. M., Smit, R. H. H., van Ommen, J. G., and Ross, J. R. H., *Stud. Surf. Sci. Catal.* **55,** 505 (1990).
5. Grasselli, R. K., and Burrington, J. D., *Ind. Eng. Chem. Prod. Res. Dev.* **23,** 393 (1984).
6. Trifiro, F., Caputo, G., and Villa, P. L., *J. Less-Common Met.* **36,** 305 (1974).
7. Sampson, R. J., and Shooter, D., *Oxid. Combust. Rev.* **1,** 223 (1965).
8. Satsuma, A., Hattori, A., Mazutani, K., Furuta, A., Miyamoto, A., Hattori, T., and Murakami, Y., *J. Phys. Chem.* **93,** 1484 (1989).
9. Dyrek, K., and Lobanowska, M., *J. Catal.* **81,** 46 (1983).
10. Ozima, M., Sato, S., and Zoltai, T., *Acta Crystallogr. Sect. B* **33,** 2175 (1977); see also JCPDS Files 31-0731, 31-0732.
11. Hanuza, J., and Jezowska-Trzebiatowska, B., *J. Mol. Catal.* **24,** 109 (1989).
12. Hardcastle, F. O., and Wachs, I. E., *J. Raman Spectrosc.* **21,** 683 (1990).
13. Chaar, M. A., Patel, D., and Kung, H. H., *J. Catal.* **109,** 463 (1988).
14. Pines, H., "The Chemistry of Catalytic Hydrocarbon Conversion." Academic Press, New York, 1981.